ISOTOPE SHIFT STUDIES
IN THE RARE EARTHS AND LEAD

Thesis by

Paul Lung Sang Lee

In Partial Fulfillment of the Requirements

for the Degree of

Doctor of Philosophy

California Institute of Technology

Pasadena, California

1972

(Submitted August 12, 1971)

ACKNOWLEDGEMENTS

I would like to thank Dr. Felix Boehm for introducing me to isotope shift studies and for his many contributions to the project. I am grateful for his guidance throughout my years in Caltech.

Drs. R. Brockmeier and R. Chesler have done the pioneering work in the field of isotope shifts and I thank them for passing to me their valuable experiences. Mr. H. Henrikson has designed the spectrometers and all special apparatus used for these experiments. I would also like to thank Mr. E. Redden for assistance in the experiments.

I wish to thank Dr. E. Seltzer for his close interest and valuable suggestions. His atomic calculations have facilitated the interpretation of the experimental results.

Financial aid from the California Institute of Technology and the U. S. Atomic Energy Commission is gratefully acknowledged.

ABSTRACT

Isotope shifts of $K_{\alpha 1}$ x-ray transitions were measured for the Neodymium isotopes Nd 142, 143, 144, 145, 146, 148 and 150, the Samarium isotopes Sm 147, 148, 149, 150, 152 and 154, the Gadolinium isotopes Gd 154, 155, 156, 157, 158 and 160, the Dysprosium isotopes Dy 162 and 164, the Erbium isotopes Er 166, 168 and 170, the Hafnium isotopes Hf 178 and 180 and the Lead isotopes Pb 204, 206, 207 and 208. A curved crystal Cauchois spectrometer was used. The analysis of the measurement furnished the variation of the mean square charge radius of the nucleus, $\delta\langle r^2\rangle$, for 23 isotope pairs. The experimental results were compared with theoretical values from nuclear models. Combining the x-ray shifts and the optical shifts in Nd and Sm yielded the optical mass shifts. An anomaly was observed in the odd-even shifts when the optical and the x-ray shifts were plotted against each other.

TABLE OF CONTENTS

TABLE OF CONTENTS (Cont'd.)

APPENDIX

LIST OF FIGURES

LIST OF TABLES

1 INTRODUCTION

The energies of atomic transitions differ slightly from one isotope of an element to the next. This isotope shift (I.S.) arises predominantly from two effects. First, there is the "Volume Effect." When a neutron is added to a nucleus, it 'dilutes' the proton distribution, causing the atomic electrons to be less tightly bound. The "Volume Effect" comes about, therefore, from the difference of the nuclear Coulomb field experienced by the atomic electron undergoing a transition. The second effect is the mass shift. The difference in the nuclear mass of the different isotopes causes a change in the kinetic energy of the nuclear mass as it recoils.

Historically, isotope shift was first observed in 1919 in optical transitions using optical interferometric techniques. Optical I.S. measurements have been continued to the present day. A review of the optical I.S. results has been compiled by Brix and Kopperman[1], and more recently by D. N. Stacey[2]. The chief limitations in this method, as far as extracting nuclear information is concerned, is the difficulties of calculating the mass shift and the electronic screening corrections.

Isotope shifts of the x-rays of muonic atoms

are being measured by several groups. Recent reviews have been prepared by Wu and Wilets[3] and by Devons and Duerdoth[4]. In these experiments, several x-rays can be measured simultaneously and therefore several moments of the charge distribution can be extracted. However, hyperfine interactions, nuclear polarization and vacuum polarization play an important role in muonic I.S. measurements and introduce uncertainties.

The present work is concerned with I.S. in atomic K x-ray. Ford and Wills[5] have shown that x-ray transition energy can be characterized by a single moment $\langle r^k \rangle$. For atomic $K_{\alpha 1}$ x-ray, to a very good approximation, k is equal to 2. Thus, x-ray I.S. can be interpreted to yield the variation of the mean square charge radius of the nucleus , $\delta\langle r^2 \rangle$. In the case of muonic x-rays, k is a function of Z. For the 2p-1s transitions, k ranges from 2 in low Z elements to 0.82 for Pb. Therefore, muonic I.S. measures $\delta\langle r^k \rangle$ where k is in most cases different from 2. The $\delta\langle r^2 \rangle$ from x-ray I.S. supplies another important parameter for the nuclear charge distribution.

High energy electron scattering experiments can be interpreted to yield $\langle r^2 \rangle$, but their absolute errors are inferior to those from x-ray I.S. experiments. The $\delta\langle r^2 \rangle$ values from x-ray I.S. can be used as a constraint

to fit the data from electron scattering experiments of different isotopes.

The first observation of $K_{\alpha 1}$ x-ray of U^{235} and U^{238} was reported in 1965 by Brockmeier, Boehm and Hatch[6]. Additional measurements have been published by Sumbaev et al[7] in Moscow and by the Caltech group[8]. The Caltech measurements were made using a 2 meter bent-curved crystal spectrometer[9]. A new 2-m bent-curved crystal spectrometer was developed for part of this work by H. E. Henrikson.

The present measurements were carried out for the Neodymium isotopes Nd 142, 143, 144, 145, 146, 148 and 150; the Samarium isotopes Sm 147, 148, 149, 150, 152 and 154; the Gadolinium isotopes 154, 155, 156, 157, 158 and 160; the Dysprosium isotopes Dy 162 and 164; the Erbium isotopes Er 166, 168 and 170; the Hafnium isotopes Hf 178 and 180, and the Lead isotopes Pb 204, 206, 207, and 208. From the data, we extracted the $\delta\langle r^2\rangle$ values of 23 isotope pairs.

The $K_{\alpha 1}$ x-ray I.S.'s are easy to interpret. Unlike muonic I.S., hyperfine interactions, nuclear polarization and vacuum polarization play insignificant roles. The main difficulty lies in the smallness of these shifts and thus in the experimental part. The fractional change in energy is of the order of 10^{-6}. In terms

of the rotation of the diffraction crystal used in these experiments, the shift is of the order of 2×10^{-7} radians. The technique developed has been applied to chemical shifts[10] where the role played by the valence electron in the chemical bonding is being probed.

2 THEORY OF THE ISOTOPE SHIFT

2.1 Survey of Volume Effect Calculation

The shift of the energies of the $1s_{1/2}$, $2s_{1/2}$, $2p_{1/2}$, $2p_{3/2}$ levels due to the change of the nuclear charge densities of different isotopes had been calculated by two approaches. The first approach was used by Racah[11], Rosenthal and Breit[12], and more recently, Wertheim and Igo[13]. They use the Dirac-Coulomb point nucleus wave functions as the starting point, and the difference in potential between a point nucleus and an extended nucleus as perturbation. Since the perturbation was not small, the calculation was not very accurate and sizeable corrections had to be applied.

The second approach made use of an exact expression derived by Broch:

$$\Delta E = \hbar c R^2 \frac{\{g_o(R)f_e(R) - g_e(R)f_o(R)\}}{\int_R^\infty \{f_o(x)f_e(x) + g_o(x)g_e(x)\}\, dx} \qquad (2.1)$$

where g_o and f_o are the relativistic Dirac-Coulomb wave functions and g_e and f_e are the wave functions which take into account the finite dimensions of the nucleus. R is the distance from the center of the nucleus outside which the potential is that of a point nucleus; the nucleus is assumed to have a sharp edge.

All calculations made the approximation that the denominator in eqn. (2.1) is equal to 1, i.e.:

$$\int_R^\infty \{ f_o(x)f_e(x) + g_o(x)g_e(x) \} dx$$

$$\approx \int_R^\infty \{ |f_e|^2 + |g_e|^2 \} dx = 1$$

The principal problem in calculating the I.S. was the determination of the correct wave functions. Various authors used different wave functions. Their results were summarized in a review article by Brix and Kopfermann[14]. A variation of the method used an integral representation for the wave functions. This had been pursued by Bodmer[15] and Fradkin[16].

All the above authors calculated the I.S. with the assumption that $E = m_o c^2$, i.e., they assumed that the binding energy of the electron was negligible compared to the electron's total energy. This assumption was not valid for x-ray I.S. Babushkin[17] calculated the x-ray I.S. using Broch's expression (eqn. 2.1) without the assumption that $E = m_o c^2$. His results represented the best calculation for x-ray I.S. up till 1969.

2.2 Present Volume Effect Calculation

The present calculation of Coulomb shift was performed by Seltzer[18]. The method used was a straightforward first order perturbation calculation using realistic electron wave functions. The shift is

$$\delta E_{vol} = -\alpha \int \delta\rho_N \left(r_N^{-1} \int_o^{r_N} \rho_e dV_e + \int_{r_N}^{\infty} \frac{\rho_e}{r_e} dV_e \right) dV_N \tag{2.2}$$

where ρ_N and ρ_e are the nuclear and electron charge distributions. For convenience in calculation, this can be rewritten

$$\delta E_{vol} = -\alpha \int \delta\rho_N \left(r_N^{-1} \int_o^{r_N} \rho_e dV_e - \int_o^{r_N} \frac{\rho_e}{r_e} dV_e \right) dV_N \tag{2.3}$$

For any reasonable nuclear charge distribution the electronic factor inside the parentheses can be expressed as an even power series in r_N.

Using a Fermi charge distribution to calculate the nuclear Coulomb potential, the electron wave functions were obtained from self-consistent field calculation. The calculation started with the Dirac equation, using the Slater free electron exchange approximation. The usual shielding effect that reduces the nuclear charge was automatically incorporated.

A Fermi charge distribution was used to calculate the nuclear Coulomb potential. For $j = \frac{1}{2}$ and $\Delta A = 2$, we can write

$$\delta E_{vol} = \sum_{n=1}^{\infty} C_n \delta\langle r^{2n} \rangle \qquad (2.4)$$

Table 1 lists the values of C_1, C_2, and C_3 for the elements measured in the present experiment.

As is shown in the next section, the dominant effect is the $C_1 \delta\langle r^2 \rangle$ term. To within an accuracy of 7% for Pb and less for the lighter elements, we can neglect the higher moments. Therefore, we can extract from the measured δE_{vol}, the mean square radial variation $\delta\langle r^2 \rangle$, i.e.:

$$\delta\langle r^2 \rangle = \delta E_{vol} / C_1$$

TABLE 1

The coefficients C_n from the self-consistent field calculations for the 1s level.

Z	C_1 meV/fm^2	C_2 meV/fm^4	C_3 meV/fm^6
Nd 60	0.238×10^3	-0.185	0.534×10^{-3}
Sm 62	0.291×10^3	-0.234	0.667×10^{-3}
Gd 64	0.351×10^3	-0.292	0.817×10^{-3}
Dy 66	0.427×10^3	-0.368	0.102×10^{-2}
Er 68	0.515×10^3	-0.463	0.128×10^{-2}
Hf 72	0.750×10^3	-0.722	0.196×10^{-2}
Pb 82	0.188×10^4	-2.110	0.559×10^{-2}

2.3 Charge Moments From Uniform Model

For the purpose of comparing experimental $\delta\langle r^2\rangle$, it is useful to calculate $\delta\langle r^2\rangle$ for a simple model. We can also calculate the higher moments and get an estimate of their relative contribution to the I.S. It has been a standard procedure to express the I.S. results in terms of a shift based on a uniformly charged sphere with radius $R_o = 1.2A^{1/3}$. We will extend the model to include deformation and calculate

$$\langle r^{2n}\rangle = \frac{\int \rho(\vec{r})\, r^{2n}\, dV}{\int \rho(\vec{r})\, dV} \tag{2.5}$$

with

$$\rho(\vec{r}) = \rho(r,\theta) = \begin{cases} \rho_o & \text{for } r/r_1 \leq 1 \\ 0 & \text{for } r/r_1 > 1 \end{cases}$$

where

$$r_1 = \bar{r}_1[1 + \beta Y_{20}(\theta)]$$

and β is the deformation parameter. To preserve the nuclear volume, $\bar{r}_1$ is chosen to be

$$R_o \left[1 + \frac{3}{4\pi}\beta^2 + \frac{1}{14\pi}\frac{5}{4\pi}\beta^3\right]^{-1/3}$$

Then we obtain

$$\delta\langle r^{2n}\rangle = \delta\langle r^{2n}\rangle_{sph} + \delta\langle r^{2n}\rangle_{def}$$

$$= \frac{2n}{2n+3} R_o^{2n} \frac{\delta A}{A} \left\{1 + \frac{n(2n+3)}{4\pi} \beta^2 + \frac{n(2n+3)^2}{42\pi} \sqrt{\frac{5}{4\pi}} \beta^3\right\}$$

$$+ \frac{3n}{4\pi} R_o^{2n} \delta(\beta^2) + \frac{n(2n+3)}{14\pi} \sqrt{\frac{5}{4\pi}} R_o^{2n} \delta(\beta^3) \qquad (2.6)$$

To see the relative contribution of the $\delta\langle r^{2n}\rangle$ to the I.S., we take the values of C_i for Pb from Table 1. We find, $C_1\delta\langle r^2\rangle$ = 366 meV, $C_2\delta\langle r^4\rangle$ = -29 meV and $C_3\delta\langle r^6\rangle$ = 4 meV.

The quantity

$$\delta E_{A^{1/3}} = C_1\delta\langle r^2\rangle_{sph} + C_2\delta\langle r^4\rangle_{sph} + C_3\delta\langle r^6\rangle_{sph} \qquad (2.7)$$

will be used later on to compare with experimental I.S.

2.4 Mass Effect

The difference in mass of the isotopes is expected to contribute to the observed x-ray I.S. This contribution can be large in the case of light nuclei, but in the case of $K_{\alpha 1}$ x-ray the mass shift amounts to only a small fraction of the of the volume shift for medium heavy and heavy nuclei.

In the c.m. system, the non-relativistic expression

for the total kinetic energy T is given by

$$T = \frac{1}{2\mu}\sum_i \vec{P}_i^{\,2} + \frac{1}{2M}\sum_{i\neq j} \vec{P}_i \cdot \vec{P}_j \qquad (2.8)$$

where μ is the reduced mass and M the nuclear mass. The first term contracts the energy level spectrum by $\frac{\mu}{m}$, (m = electron mass) the usual reduced mass effect.

The second term gives rise to the "specific mass shift." In optical transitions, where one has to deal with a large number of transitions, the calculation of the "specific mass shift" is very difficult[19]. This is a source of difficulty in interpreting optical I.S. data.

In the case of x-ray I.S., the overlap between the outer shells with electrons in the K and L_{III} shells is small and the "specific mass shift" can be calculated reliably. Chesler[20] has calculated the effect for the $K_{\alpha 1}$ transition for Z = 42, 50, 62, 74 using the radial wave functions of Herman and Skillman[21] in a method similar to that due to Vinti[22]. Chesler's calculation shows that the $K_{\alpha 1}$ mass shift depends essentially on the core electrons and hence, varies smoothly as Z and is numerically equal to -0.3 of the reduced mass shift. The total mass shift is given by

$$\delta E_M = -\frac{2}{3}\left(\frac{\delta A}{1836\bar{A}^2}\right) E_{K_{\alpha 1}} \qquad (2.9)$$

where $\bar{A}$ and δA are the average mass number and neutron difference for the isotope pair, and $E_{K_{\alpha 1}}$ is the energy of the $K_{\alpha 1}$ x-ray.

Table 2 lists the mass shifts for the isotope pairs measured. Their magnitude is of the order of 2% of the total shift.

Since δE_M has a negative sign, the measured shift is smaller than what the "Volume shift" alone should be. Thus to get the "Volume shift" we add the absolute value of δE_M to the measured value.

TABLE 2

Total Mass shifts for the Isotope pairs measured

Isotope Pair	Total Mass Shift (meV)
Nd 142-143	-0.7
Nd 142-144	-1.3
Nd 144-145	-0.6
Nd 144-146	-1.3
Nd 146-148	-1.2
Nd 148-150	-1.2
Sm 147-148	-0.7
Sm 148-149	-0.7
Sm 148-150	-1.3
Sm 150-152	-1.3
Sm 152-154	-1.2
Gd 154-155	-0.7
Gd 154-156	-1.4
Gd 156-157	-0.6
Gd 156-158	-1.2
Gd 158-160	-1.2
Dy 162-164	-1.2
Er 166-168	-1.3
Er 168-170	-1.3
Hf 178-180	-1.3
Pb 204-206	-1.3
Pb 206-207	-0.6
Pb 206-208	-1.3

3 EXPERIMENTAL SYSTEMS

3.1 Experimental Method

The precision measurements of the differences of the $K_{\alpha 1}$ x-rays of different isotopes were done with the bent-curved crystal spectrometer in the Cauchois geometry. This method was first used by Sumbaev and Mezentsev[23].

The fluorescent x-rays from an isotope sample were Bragg refracted at the bent crystal and were focused at a narrow receiving slit. The x-rays were detected by a scintillation detector behind the slit. The x-ray profiles were scanned by moving the spectrometer in discrete steps. The output was stored in a magnetic tape. The spectrometer was programmed for automatically scanning the $K_{\alpha 1}$ region in a repetitive fashion.

Two independent experimental arrangements were used for these experiments. Arrangement I used an x-ray tube to excite fluorescent x-ray. The x-ray profile was scanned by moving the crystal block in fixed increments. Arrangement II used 200 Ci Yb^{169} as the source of excitation. In this arrangement, the crystal block was fixed for a given x-ray and the scanning was accomplished by moving the receiving

slit.

A plot of the natural line width of the x-ray versus Z together with the constant instrumental width ($\Delta\lambda$ = 0.2 x.u.) is shown in fig. 1. It can be seen that the widths are of comparable values. Also shown in fig. 1 is the I.S. calculated from a uniform spherical charge model. In terms of the natural line width, the shifts are a few parts in a thousand.

3.2 Arrangement I: X-ray Source and Spectrometer

Fluorescent $K_{\alpha 1}$ x-rays were excited by bombarding the isotope samples with the bremstrahlung x-ray from a medical x-ray tube. The tube was operated at 155 KeV and 15 mA with a ¼" aperture at the output window to minimize background.

The spectrometer was designed by H. Henrikson and is described in detail in Ref. 9 . A schematic diagram of the experimental arrangement is shown in fig. 2.

The bremstrahlung from the x-ray tube fell on one of the samples on the sample wheel. A small motor rotated the sample at the rate of 10 rpm to average angular target inhomogeneities. The fluorescent x-rays to be measured went through the lead tunnel which was set at the correct Bragg angle θ with respect to the

Figure 1. Natural and instrumental linewidths in the present experiments versus the atomic number. For comparison, the two neutron isotope shift calculated with the uniform spherical charge model (Eqn. 2.7) is also shown.

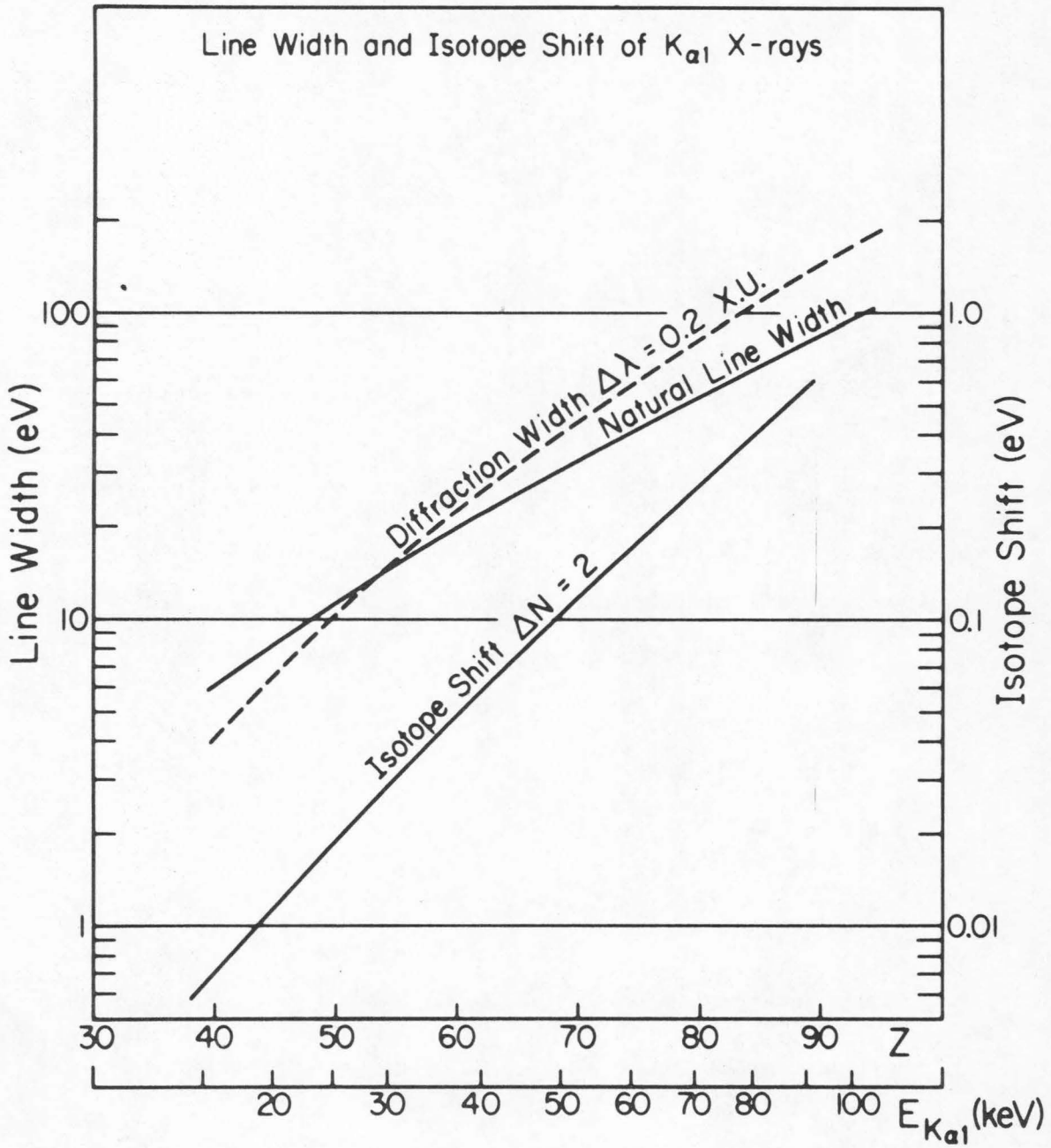
Line Width and Isotope Shift of $K_{\alpha 1}$ X-rays
Line Width (eV)
Isotope Shift (eV)
100
10
1
1.0
0.1
0.01
Diffraction Width $\Delta\lambda = 0.2$ X.U.
Natural Line Width
Isotope Shift $\Delta N = 2$
30
40
50
60
70
80
90
Z
20
30
40
50
60
70
80
100
$E_{K\alpha 1}$ (keV)

FIG. 1

crystal. After being diffracted at the bent crystal, the x-ray was focused into the receiving slit (and was then detected by the NaI detector). The receiving slit was adjusted to be at a distance 2 x cos θ meters. The width of the slit was set to be 0.2 mm.

Usually to scan a region with a Cauchois spectrometer we had to move the crystal, and either the source or the detector simultaneously in order to preserve the condition for Bragg diffraction. In the present experiment, the scanning was over a region of 1 minute of arc only. Since for our small x-ray source only a small portion of the crystal was in Bragg condition, this slight difference in angle was automatically accommodated by a slightly different portion of the crystal, with the result that moving the crystal block was sufficient.

The crystal pivot was linked to a precision sine screw assembly. A Slo-syn stepping motor drove the sine screw through discrete steps. Each step corresponded to a change of 10 m.x.u. in wavelength. The Slo-syn motor was controlled by a modified Slo-syn Indexer which advanced the spectrometer in steps of 30 m.x.u. until the spectrometer had reached the end of the x-ray profile. Then the Indexer would step the crystal block to its original position. The details

of the spectrometer control system is given in Appendix I.

The output from the NaI detector was amplified and went through a single channel analyser before it got into a scaler. A crystal based master timer controlled the electronic system and after each twenty seconds period the six digit number from the scaler was transferred through a magnetic tape scanner to a magnetic tape. The counting rate at the peak was of the order of 2000 counts/sec.

3.3 Arrangement II: Yb^{169} Source and Spectrometer

Using an x-ray tube to excite fluorescent x-ray had several drawbacks. Since only x-rays with energy above the K edge contributed to excitation, a large part of the bremstrahlung output was unused. On the practical side, there were many problems connected with operating an x-ray tube on a continuous basis. The voltage, in particular the x-ray filament voltage, had to be stabilized. The rectifier diodes had a guaranteed life time of 2000 hours and were a source of financial strain.

A radioactive source would solve the problem of stability and maintenance. By choosing a source which had an energy around the K edge, excitation could be greatly enhanced. Consequently, we could cut down on the running time of an experiment.

Figure 2. Cauchois spectrometer and control system.

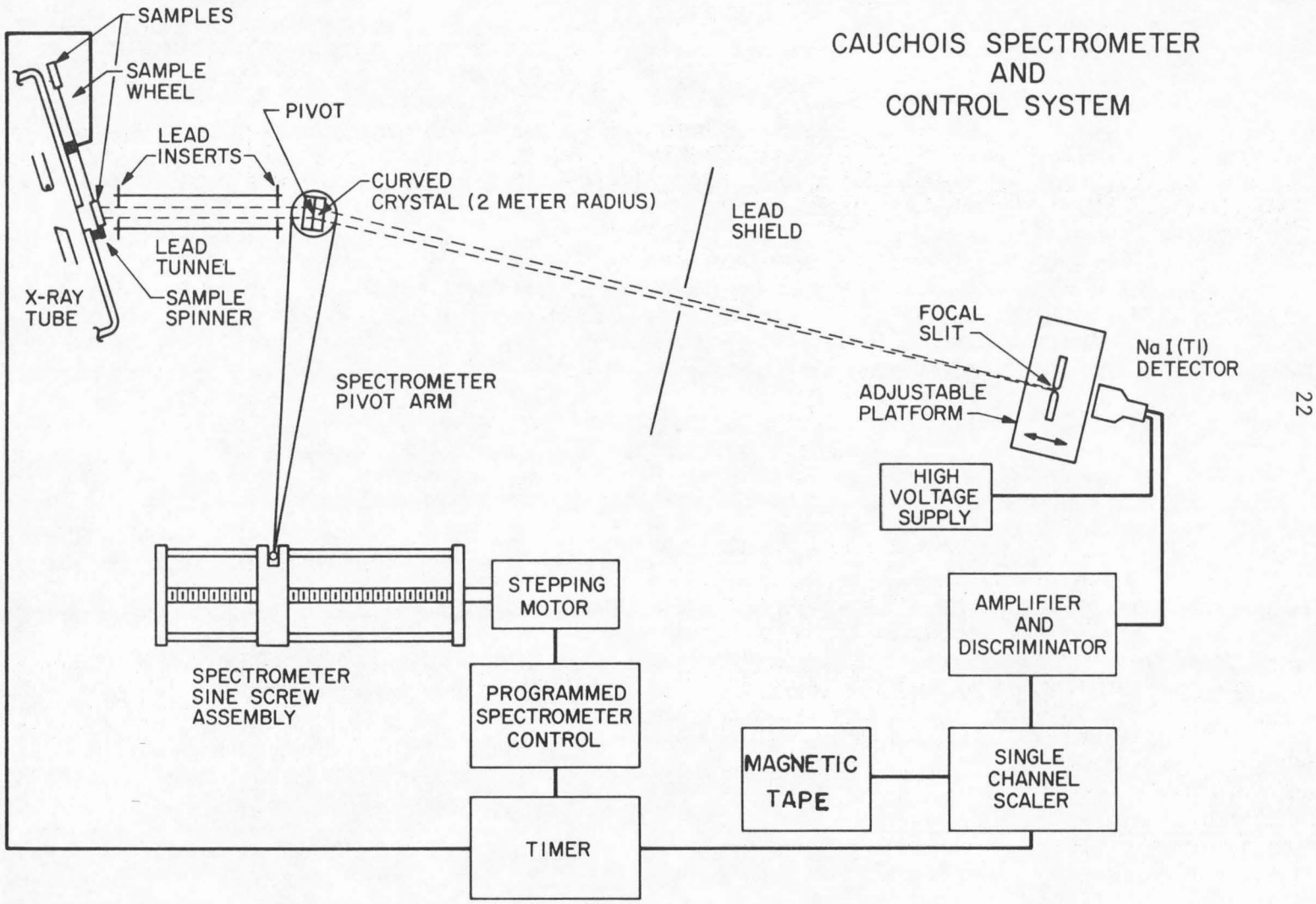
CAUCHOIS SPECTROMETER
AND
CONTROL SYSTEM
SAMPLES
SAMPLE WHEEL
PIVOT
LEAD INSERTS
CURVED CRYSTAL (2 METER RADIUS)
LEAD SHIELD
LEAD TUNNEL
X-RAY TUBE
SAMPLE SPINNER
FOCAL SLIT
NaI(Tl) DETECTOR
SPECTROMETER PIVOT ARM
ADJUSTABLE PLATFORM
HIGH VOLTAGE SUPPLY
STEPPING MOTOR
AMPLIFIER AND DISCRIMINATOR
SPECTROMETER SINE SCREW ASSEMBLY
PROGRAMMED SPECTROMETER CONTROL
MAGNETIC TAPE
SINGLE CHANNEL SCALER
TIMER

FIG. 2

The difficulty with a radioactive source was the shielding required for a strong source.

There were several factors governing the choice of a source that would be suitable for the experiment. The important considerations were:

1) A significant amount of the radiation had to be in the energy range for fluorescent excitation.

2) The half life had to be long so that frequent rejuvenation was not necessary.

3) The neutron absorption coefficient must be high, so that a strong source could be produced in a short time in the reaction. Otherwise, the cost would be exorbitant.

4) The isotope to be activated must not be excessively expensive.

A search was made with the above requirements in mind. The final choice was Yb^{169}. It has a 63 KeV γ line with a half life of 31 days. The neutron absorption coefficient for Yb^{168} is 5500 barnes. Two hundred mg. of 20% enriched Yb^{168} was obtained from Oak Ridge. This amount of Yb powder was mixed with 400 mg. of Al powder and sent to the G.E. Vallecitos Nuclear Center in a capsule. Irradiating for 15 days at a flux of 1.1×10^{14} gave a source of 200 Ci activity. The Yb^{169} capsule was enclosed in a container with a shutter

in front (see fig. 3). The shutter could be removed by remote control and the capsule pushed up so that it was flush with an isotope sample.

The spectrometer used was designed by H. Henrikson. It consisted of two separate units: 1) the crystal pivot and 2) the movable slit. These two units rested on a massive octahedral concrete support and were placed 2 meters apart. The fluorescent x-rays were Bragg refracted at the crystal and were detected by a NaI detector behind the slit. (See fig. 4)

The crystal pivot unit contained the bent crystal, the pivot bearing and a screw mechanism which moved the crystal for each x-ray line. For the experiment, the 310 plane of a 2 mm. thick quartz crystal bent to a radius of 2 meters was used.

Instead of a precision sine screw to move the crystal block, we used a commercial micrometer screw connected to a Bodine motor. During an experiment, the crystal remained stationary. It was only moved when x-rays from another element were tuned in.

The scan of the x-ray profile was achieved by moving linearly the receiving slit. The slit platform was mounted on two sheet springs which constrained the slit to move perpendicular to the x-ray beam. The spring also served to reduce inertia when the slit was

Figure 3. Yb^{169} source container. To bring the source to position, the bar with hole is slid so that the hole is right in front of the source capsule. The plunger is then remotely moved in until the source is flush with the front plate which has a hole in the middle.

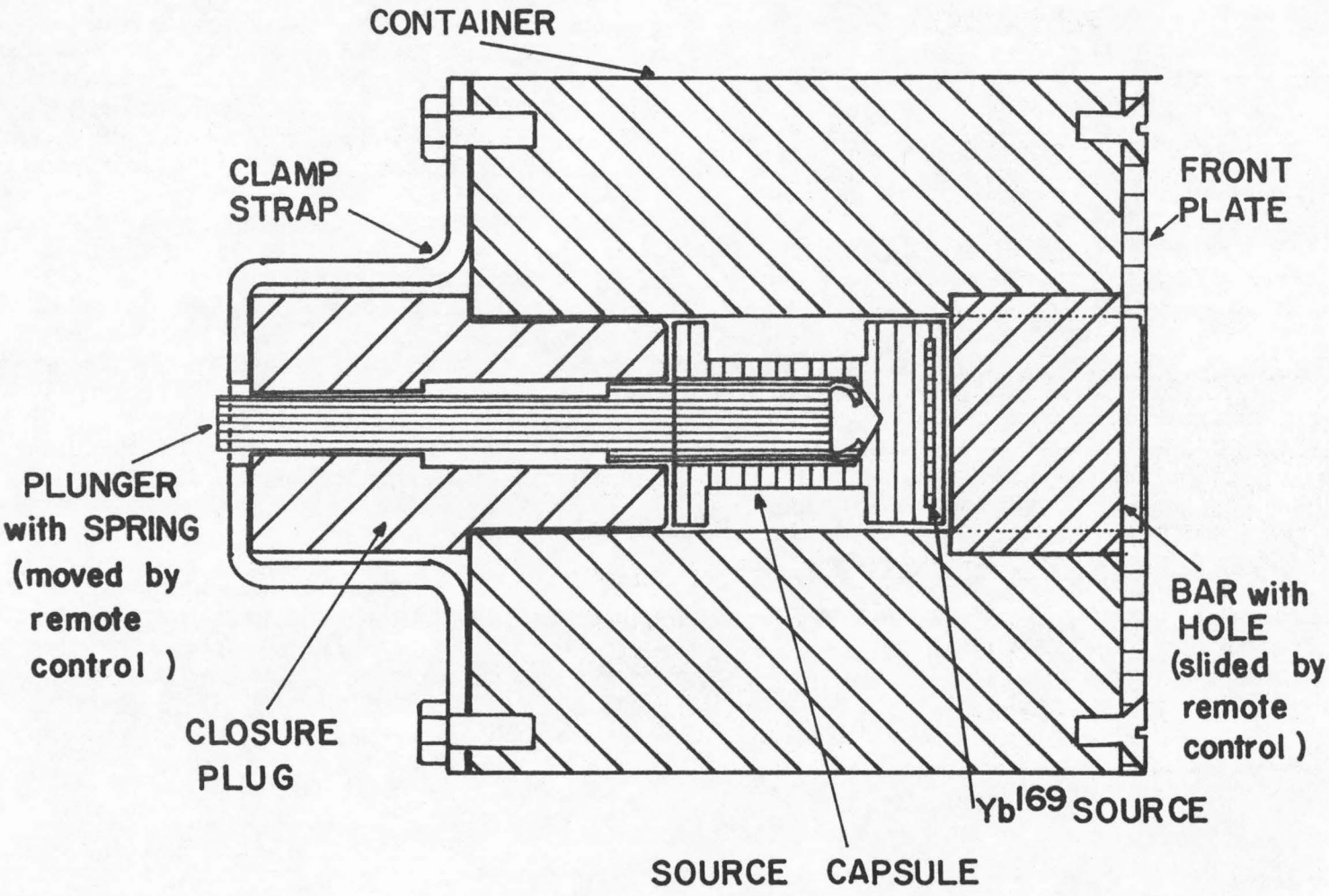

Yb^{169} SOURCE CONTAINER

FIG. 3

moved in discrete steps. The slit platform was rigidly connected to one part of the precision ten thousandth inch micrometer.

The micrometer was coupled to a Slo-syn motor with 200 steps per revolution. Eight steps constituted a movement of the slit of 0.001". The movement of the slit is directly related to the change in wavelength.

$$\delta\lambda \text{ (m.x.u.)} = \frac{2d}{D}\,\delta x = \frac{30 \text{ m.x.u.}}{0.001"}\,\delta x$$

where $d = 1.1738$ Å is the lattice spacing of the 310 plane of the quartz crystal and $D = 200$ cm. is the diameter of the Rowland circle. So a slit movement of 0.001" corresponded to 30 m.x.u.

The spectrometer was placed in an enclosed room and the temperature was kept within $0.1^{\circ}C$. The slit mechanism was tested by measuring the center of the 63 KeV γ line of Yb^{169}.

The circuitry for the spectrometer control system and the electronics for x-ray detection were similar to that of system I. The details are given in Appendix I.

4 EXPERIMENTAL PROCEDURE

4.1 Sample Preparation

The isotope samples were obtained on loan from Oak Ridge National Laboratory. They came usually in the form of oxides. Crystallographic analysis was made on each sample, using a Guinier Camera, to ensure that the isotopes for the same element had the same crystal structure. In the case of Nd, the isotopes had to be converted from Nd_2O_3 to NdF_3 to bring them to the same crystal structure; while in the case of Pb, the isotopes had to be converted from $Pb(NO_3)_2$ to PbS.

Since we used an extended source, some x-rays would impinge on the crystal planes with a small vertical angle. This gave rise to a vertical divergence shift. In order that the shifts were identical for all isotope samples, the samples had to be prepared in an identical fashion. To minimize the vertical divergence effect, we chose the sample thickness such that the change in counting rate versus thickness was a minimum. In this way, slight variation in thickness over the sample area became tolerable. Any angular variation was averaged out by rotating the samples during the experiment.

The appropriate amount of the isotope was mixed

Figure 4. Experimental arrangement II.

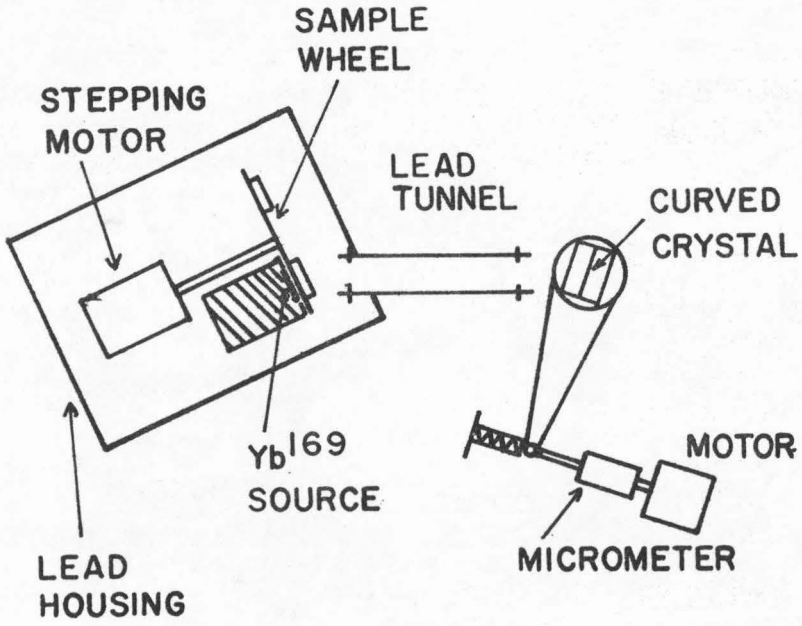

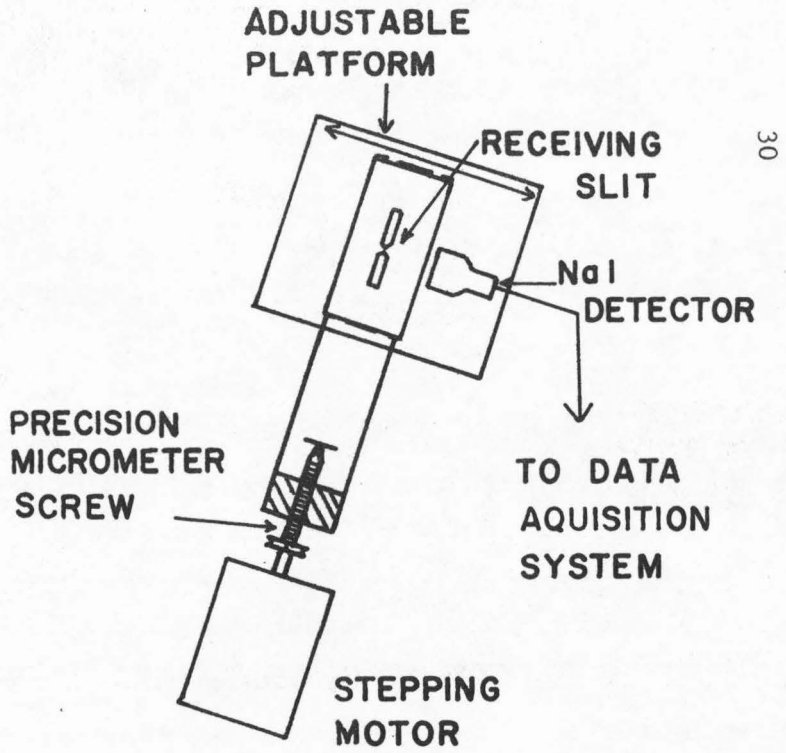

EXPERIMENTAL ARRANGEMENT II

FIG. 4

with an organic substance and the mixture was put in a press. The resulting pill was self supporting. Depending on the compound, we used different organic substances. The details of this process is given in Appendix II.

The isotope sample, in the form of a pill, was placed inside a holder. Up to four such holders could be put on the sample wheel in front of the source of excitation, i.e. the x-ray tube window in arrangement I and the Yb^{169} source in arrangement II.

4.2 Data Aquisition

Since the shifts we were measuring were of the order of a few thousandths of the natural line width of the x-ray, it would be far beyond present experimental technique to deduce the shifts from independent absolute measurements of the wavelengths of the $K_{\alpha 1}$ x-ray of the different isotopes. Instead, we compared the x-rays almost simultaneously and deduced the energy difference from each run.

The $K_{\alpha 1}$ line was scanned in steps of 30 m.x.u. At the end of each step, the fluorescent x-rays from one isotope sample were detected by a NaI scintillation detector and got counted in 20 seconds. Then the sample wheel was turned to bring the next isotope

TABLE 3

Counting pattern for three isotopes A, B, C and 31 spectrometer positions. Beginning at position 1, we measure A, then B, C, and again A, each for 20 seconds. We move to position 2 and measure B, C, A, and B. This goes on until we come to the 31st position. The spectrometer is then moved to position 1 again for scan 2. After three scans we complete the pattern in this table. The counts belonging to each isotope are summed for each position to form a "data unit" for the least squares analysis.

Spectrometer Position / Scan	1	2	...	31
1	A,B,C,A	B,C,A,B		A,B,C,A
2	B,C,A,B	C,A,B,C	...	B,C,A,B
3	C,A,B,C	A,B,C,A		C,A,B,C
Data Unit	ΣA, ΣB, ΣC	ΣA, ΣB, ΣC	...	ΣA, ΣB, ΣC

sample into position. After all the isotope samples had been measured, we returned to the first isotope sample for another measurement before we moved the spectrometer to the next position. At the end of the scan, the spectrometer was moved automatically back to the starting position and the process repeated. X-ray counts that corresponded to the same isotope for the same position from several scans were summed before they were analysed. The number of positions was chosen according to the width of the x-ray and also to ensure that each isotope was counted for equal time. A counting pattern for three isotopes is shown in Table 3.

A dead time timer controlled the system during the isotope changing interval. This timer was set to be 6 seconds. For running simultaneously four isotopes over a profile width of typically 1 x.u., the total time for one data unit was around 4½ hours. To make a measurement with an uncertainty around 5%, it required about 100 data units. Therefore, the running time required to measure the I.S. of four isotopes was about 20 days.

4.3 Data Analysis

The raw data were stored in magnetic tapes. They were taken out at intervals of two to three days and

analysed in the Caltech Computing Center. The first step in the analysis was to group the data points into data units. Each data unit contained one set each of the x-ray profiles of each isotope. These profiles were then separately fitted with a five parameter Gaussian with sloping background in a least squares program. The five parameters were peak height, half-width, center, background and slope of background. Fig. 5 shows a typical profile from one data unit and its least squares fit.

The line shift for each data unit was computed from the differences of the center parameter values of the different isotopes. From a large number of such shifts we computed the average and the standard deviation.

In cases where we had a series of isotopes, more combinations than the number of isotopes were measured. The results were checked against each other for consistency. A linear least squares fit was performed to yield the best values and the uncertainties of the I.S. for all the combinations.

After we had combined all experimental values, we obtained the energy shifts from one of our isotope samples to another. Since the samples were not pure isotopes, we had to take the isotopic composition into account before we would get the I.S. However, in most

Figure 5. Profile of x-ray.

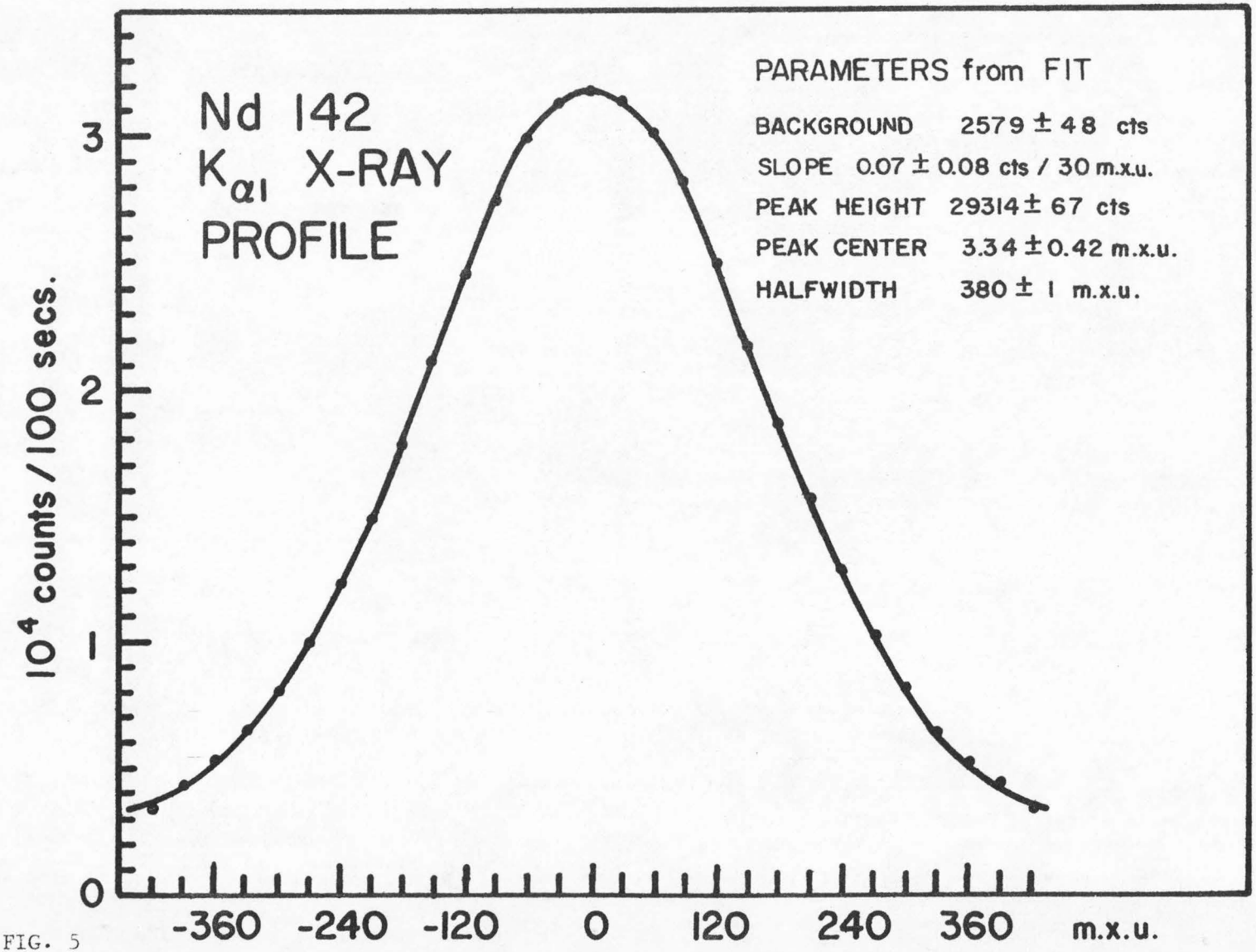
Nd 142
$K_{\alpha 1}$ X-RAY
PROFILE
PARAMETERS from FIT
BACKGROUND 2579 ± 48 cts
SLOPE 0.07 ± 0.08 cts / 30 m.x.u.
PEAK HEIGHT 29314 ± 67 cts
PEAK CENTER 3.34 ± 0.42 m.x.u.
HALFWIDTH 380 ± 1 m.x.u.
10^4 counts / 100 secs.
0
1
2
3
-360
-240
-120
0
120
240
360
m.x.u.

FIG. 5

cases, this was a correction of only a few percent.

In cases where we had measured all the isotopes, an exact inversion could be made to give the isotopic correction coefficient. In other cases, we used the relative I.S. from optical I.S. measurements. Appendix III outlines this procedure.

From these I.S. values we subtracted the contributions of the mass shift given in Table 2. This gave us the final values for the Volume Shift.

The systematic error that came from vertical divergence effects and from crystal imperfection was assigned to be ±0.01 m.x.u.[25] This error was added to all the experimental errors.

5 RESULTS

The earlier experiments were performed for two isotopes at the same time. The number of combinations measured was more than the number of isotopes, so the isotope shifts were overdetermined. This afforded a check on the consistency of the experiment. To get the final result, these values were combined in a linear least squared fit.

In the case of Sm, PbS and NdF_3, more than two isotopes were mounted on the sample wheel at the same time. So we were measuring several shifts at each run. These sets of shifts were also combined at the end. All the experimental measurements are listed in Appendix IV.

We present in Table 4 the summary of the I.S. results. The values are the best values of the I.S. for the isotopes pair. They represent the combined total of all measurements except in the case of Pb. The $Pb(NO_3)_2$ samples were prepared under heat. There was some uncertainty that decomposition might have taken place. So even though the I.S. values were not drastically different from the values from PbS, we did not include them.

The Volume Shifts in column 2 is the final value

after applying isotopic composition correction, and mass shift correction. For comparison, we list in column 3 the shift expected for a spherical nucleus with uniform charge,

$$\delta E_{A^{1/3}} = C_1 \delta\langle r^2\rangle_{sph} + C_2 \delta\langle r^4\rangle_{sph} + C_3 \delta\langle r^6\rangle_{sph}$$

(see section 2.3)

Also included in Table 4 are the $\delta\langle r^2\rangle$ values. Column 4 gives the experimental $\delta\langle r^2\rangle = (\delta E)_{exp}/C_1$ (section 2.2). $\delta\langle r^2\rangle_{sph}$ and $\delta\langle r^2\rangle_{def}$ (section 2.3) for a uniform charge model are tabulated in columns 5 and 6 for comparison.

In calculating $\delta\langle r^2\rangle_{def}$, for even A nuclei we use β values deduced from B(E2) values given in Ref. 24. Since the B(E2) values have errors of about 5%, the $\delta\beta^2$ values have errors of 7%. This gives an error of about 35% in $\delta\langle r^2\rangle_{def}$. For odd A, the uncertainty is even bigger.

TABLE 4

Final results.

Isotope Pair	Experimental Coulomb Shift δE (meV)	δE_{sph} (meV)	Experimental $\delta\langle r^2\rangle = \delta E/C_1$ (fm^2)	Uniform Charge Model $\delta\langle r^2\rangle_{sph}$ (fm^2)	Uniform Charge Model $\delta\langle r^2\rangle_{def}$ (fm^2)
Nd 142-143	21.1 ± 2.2	25.3	0.089 ± 0.009	0.111	-0.142
Nd 142-144	70.0 ± 3.7	50.9	0.294 ± 0.016	0.222	0.002
Nd 144-145	6.5 ± 4.5	25.2	0.027 ± 0.019	0.110	-0.152
Nd 144-146	55.4 ± 7.7	50.8	0.233 ± 0.033	0.221	0.076
Nd 146-148	61.5 ± 4.5	50.7	0.258 ± 0.019	0.221	0.180
Nd 148-150	100.7 ± 3.6	51.7	0.423 ± 0.015	0.223	0.409
Sm 147-148	49.8 ± 2.9	30.4	0.171 ± 0.010	0.109	0.252
Sm 148-149	23.3 ± 2.3	30.4	0.080 ± 0.008	0.109	-0.253
Sm 148-150	88.3 ± 3.0	61.4	0.303 ± 0.010	0.220	0.117
Sm 150-152	119.5 ± 3.5	62.1	0.411 ± 0.012	0.222	0.614
Sm 152-154	64.3 ± 3.8	63.3	0.221 ± 0.013	0.226	0.349
Gd 154-155	39.2 ± 8.1	37.4	0.112 ± 0.024	0.111	0.200
Gd 154-156	71.4 ± 8.1	74.8	0.203 ± 0.023	0.223	0.272
Gd 156-157	10.4 ± 4.4	37.4	0.030 ± 0.013	0.112	-0.065
Gd 156-158	50.6 ± 3.6	75.1	0.144 ± 0.010	0.224	0.200
Gd 158-160	54.0 ± 3.4	74.9	0.154 ± 0.010	0.224	0.066
Dy 162-164	55.7 ± 4.3	89.9	0.130 ± 0.010	0.222	0.105

TABLE 4 (cont'd)

Final results.

Isotope Pair	Experimental Coulomb Shift δE (meV)	δE_{sph} (meV)	Experimental $\delta\langle r^2\rangle = \delta E/C_1$ (fm^2)	Uniform Charge Model $\delta\langle r^2\rangle_{sph}$ (fm^2)	Uniform Charge Model $\delta\langle r^2\rangle_{def}$ (fm^2)
Er 166-168	69.5 ± 4.5	107.3	0.135 ± 0.009	0.220	-0.016
Er 168-170	80.0 ± 6.1	106.7	0.155 ± 0.012	0.219	-0.081
Hf 178-180	77.4 ± 5.3	149.3	0.103 ± 0.007	0.211	-0.027
Pb 204-206	183.3 ± 38.7	342.5	0.098 ± 0.021	0.196	-0.011
Pb 206-207	49.2 ± 19.8	170.8	0.026 ± 0.011	0.097	-0.017
Pb 206-208	189.4 ± 23.7	341.3	0.101 ± 0.013	0.195	-0.017

6 DISCUSSION OF RESULTS

6.1 Comparison with Other X-ray Isotope Shifts

X-ray I.S.'s were measured in some isotopes of Mo, Ba, Nd, and Sm by Sumbaev[26]. In the case of Nd and Sm, a direct comparison with our result and Sumbaev's is possible.

We list here both our results on Nd:

Nd	δE(meV)	
	Sumbaev[26]	This Work
144-146	64 ± 11	55.7 ± 7.7
146-148	66 ± 10	61.5 ± 4.5
148-150	111 ± 13	100.7 ± 3.6

In the case of Sm our results are:

Sm	δE(meV)	
	Sumbaev[26]	This Work
148-150	102 ± 15	88.3 ± 3.0
150-152	110 ± 16	119.5 ± 3.5

The overall agreement is excellent. In all cases, the measurements agree within their error limits.

Van Eijk and Visscher[27] have reported a measurement of the x-ray I.S. in Ce^{140}-Ce^{142}. Van Eijk and

Schutte[28] have measured Dy^{162}-Dy^{164} using a curved crystal spectrometer in the DuMond geometry. Their value for δE_{Vol} is 58.1 ± 3.3 meV. This is in excellent agreement with our value of 55.7 ± 4.3 meV.

6.2 Comparison with Optical Isotope Shift

In section 2.2 we have written the I.S. as follows:

$$\delta E_{Vol} = \sum_{n=1}^{\infty} C_n \delta\langle r^{2n}\rangle$$

$$= C_1 \left\{ \sum_{n=1}^{\infty} \frac{C_n}{C_1} \delta\langle r^{2n}\rangle \right\}$$

$$\equiv C_1 \lambda \qquad (6.1)$$

According to the calculations by Seltzer[18], the ratios C_n/C_1 are largely independent of the principal quantum numbers. The change in C_2/C_1 in going from 1s to 2s is only a few tenths of a percent. The change is even less when we go beyond the 2s level. This means that both optical I.S. and x-ray I.S. measure the same nuclear parameter

$$\lambda = \delta\langle r^2\rangle + \frac{C_2}{C_1} \delta\langle r^4\rangle + \frac{C_3}{C_1} \delta\langle r^6\rangle + \ldots \qquad (6.2)$$

In x-ray I.S. we measure $\delta E = \delta E_{Vol} + \delta E_M$ and

after calculating δE_M we obtain $\lambda = \delta E_{Vol}/C_1$.

For an I.S. of an optical transition i for isotopes of mass numbers A and A', the quantity measured is:

$$\delta E^{i,A,A'} = \delta E_{Vol}{}^{i,A,A'} + \delta E_M{}^{i,A,A'}$$

$$= C_1^i \lambda + \frac{M^i(A - A')}{AA'} \qquad (6.3)$$

Here the coefficients C_1^i and M^i depend on the electronic configuration. Even though many optical lines can be measured, the coefficients C_1^i and M^i cannot be evaluated.

By using the x-ray I.S. results, however, we can extract C_1^i and M^i. To do that we substitute the $\delta E_{Vol}/C_1$ for x-ray into eqn. 6.3 and get

$$\delta E^{i,A,A'} = \frac{C_1^i}{C_1} \delta E_{Vol} + \frac{M^i(A - A')}{AA'}$$

We can rewrite this as:

$$\left[\left(\frac{AA'}{A - A'}\right) \delta E^{i,A,A'}\right] = \frac{C_1^i}{C_1}\left[\left(\frac{AA'}{A - A'}\right) \delta E_{Vol}\right] + M^i \qquad (6.4)$$

Therefore, by plotting values of optical shifts times $\frac{AA'}{A - A'}$ versus the values of x-ray I.S. times $\frac{AA'}{A - A'}$ for different isotope pairs, we should get a

straight line. The slope of this line gives us C_1^i and the intercept will yield M^i.

This method of comparison is particularly useful for cases where many isotope pairs are measured. We have made the comparison in the case of Nd and Sm.

Hansen et al.[29] have made an exhaustive study of optical I.S. for five optical lines in Nd. No information about the nuclear parameter λ (eqn. 6.2) can be extracted because C_1^i and M^i were unknowns.

A plot of the optical I.S. versus the x-ray I.S. values is shown in fig. 6 for three optical lines in Nd. Two sets of straight lines are shown. The solid lines denote the best fit to the even-even shifts while the dotted lines are the best fits to all the shifts. It can be seen that the odd isotopes do not follow the straight line predicted by eqn. 6.4. Faessler and Walther[30] have proposed that this discrepancy is due to the polarization of the atomic electron by the magnetic dipole moment. Since the question is open, we have only used the even-even shift to deduce C_1^i and M^i. These values are presented in Table 5 for the five optical lines. Using these values of C_1^i and M^i we deduced the $\delta\langle r^2\rangle$ values. These values are also shown in Table 5.

A similar comparison is carried out for the case

TABLE 5

Optical Line λ^i(Å)	$M^i \cdot 10^{-5}$ (mK x nucleon)	Total Mass Shift per Nucleon (mK)	C_1^i (mK/fm^2)
4484	2.9 ± 0.5	-13 ± 2.4	-27 ± 11
4897	2.2 ± 0.3	-10 ± 1.4	-19 ± 12
4924	2.8 ± 0.3	-13 ± 1.4	-16 ± 11
4945	1.3 ± 0.6	-6.3 ± 2.9	-27 ± 5
5621	1.6 ± 0.2	-7.5 ± 1.1	+130 ± 22

Isotope Pair	142-144	144-146	146-148	148-150	142-143	144-145
$\delta\langle r^2\rangle$	0.284 ± 0.009	0.265 ± 0.010	0.293 ± 0.008	0.402 ± 0.015	0.132 ± 0.030	0.111 ± 0.025

Optical total mass shifts per nucleon and $\delta\langle r^2\rangle$ for Nd as derived from a comparison of the optical (Ref. 29) and x-ray even-even isotope shifts. M^1 and C_1^1 are defined in eqn. (6.3). The $\delta\langle r^2\rangle$ values were obtained from an analysis of the x-ray lines and the 4945 and 5621 Å lines. The normal mass shift per nucleon is -0.5 mK.

Figure 6. Comparison of the x-ray volume shift and the optical shifts in Nd. Fits are shown for two alternatives, even isotopes only (drawn lines) and all isotopes (dotted lines).

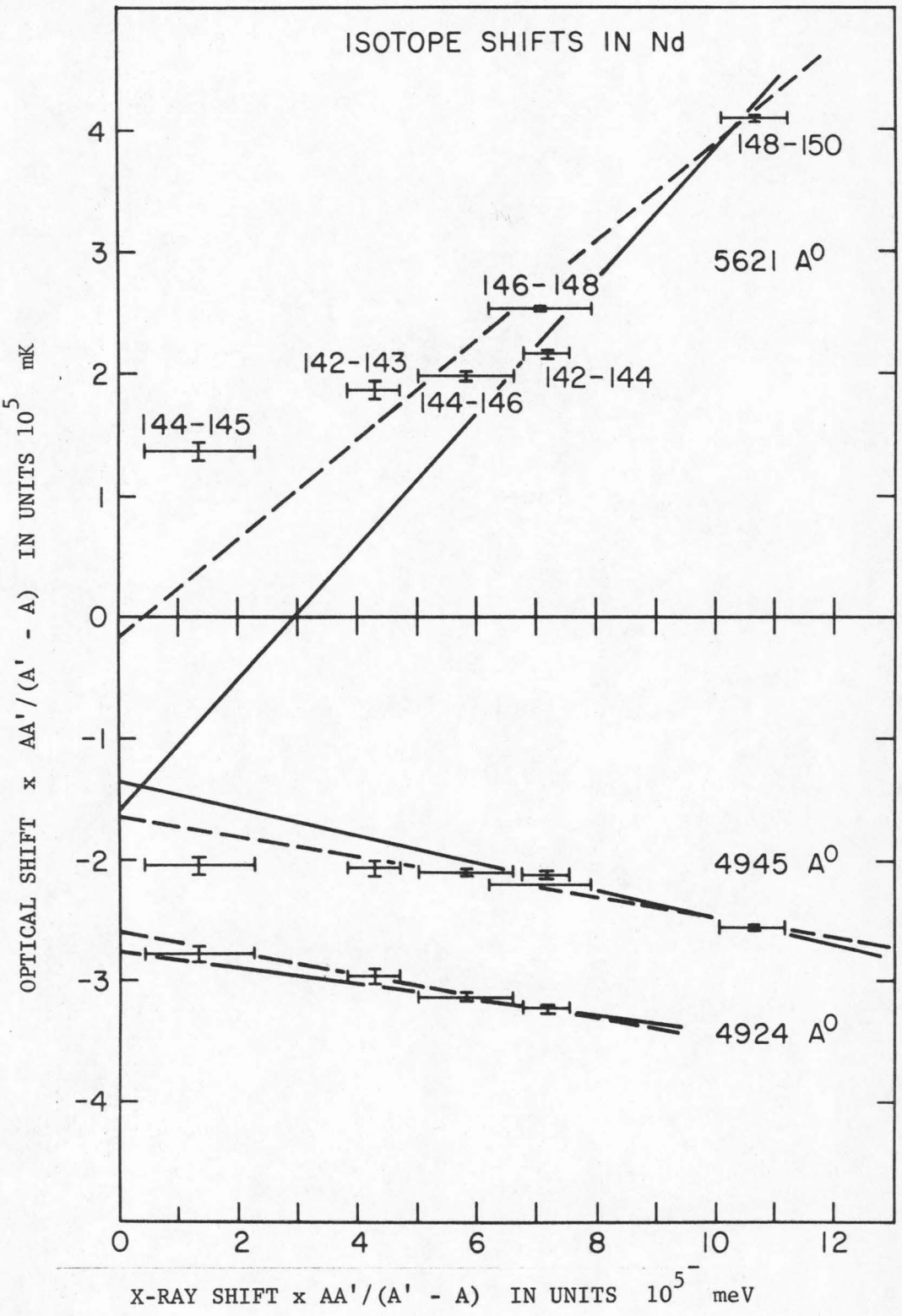
ISOTOPE SHIFTS IN Nd
148-150
5621 A⁰
146-148
142-143
142-144
144-146
144-145
4945 A⁰
4924 A⁰
OPTICAL SHIFT x AA'/(A' - A) IN UNITS 10⁵ mK
X-RAY SHIFT x AA'/(A' - A) IN UNITS 10⁵ meV
4
3
2
1
0
-1
-2
-3
-4
0
2
4
6
8
10
12

FIG. 6

TABLE 6

Optical Line in Sm	Opt. Mass Shift $M^i \times 10^{-5}$ (mK x Nucleon)	Electronic Factor C_1^i (mK/fm^2)
4910 Å	0.04 ± 0.03	-9.2 ± 0.9
5088 Å	-0.14 ± 0.61	-174 ± 17
5175 Å	2.1 ± 0.8	240 ± 24
5252 Å	2.4 ± 1.0	281 ± 27
5271 Å	1.7 ± 0.6	162 ± 15

Optical mass shifts M^i and electronic factor C_1^i for different optical transitions reported in Ref. 29 as derived from a comparison of optical and x-ray isotope shifts.

Figure 7. Comparison of the x-ray volume shifts and the optical shifts in Sm.

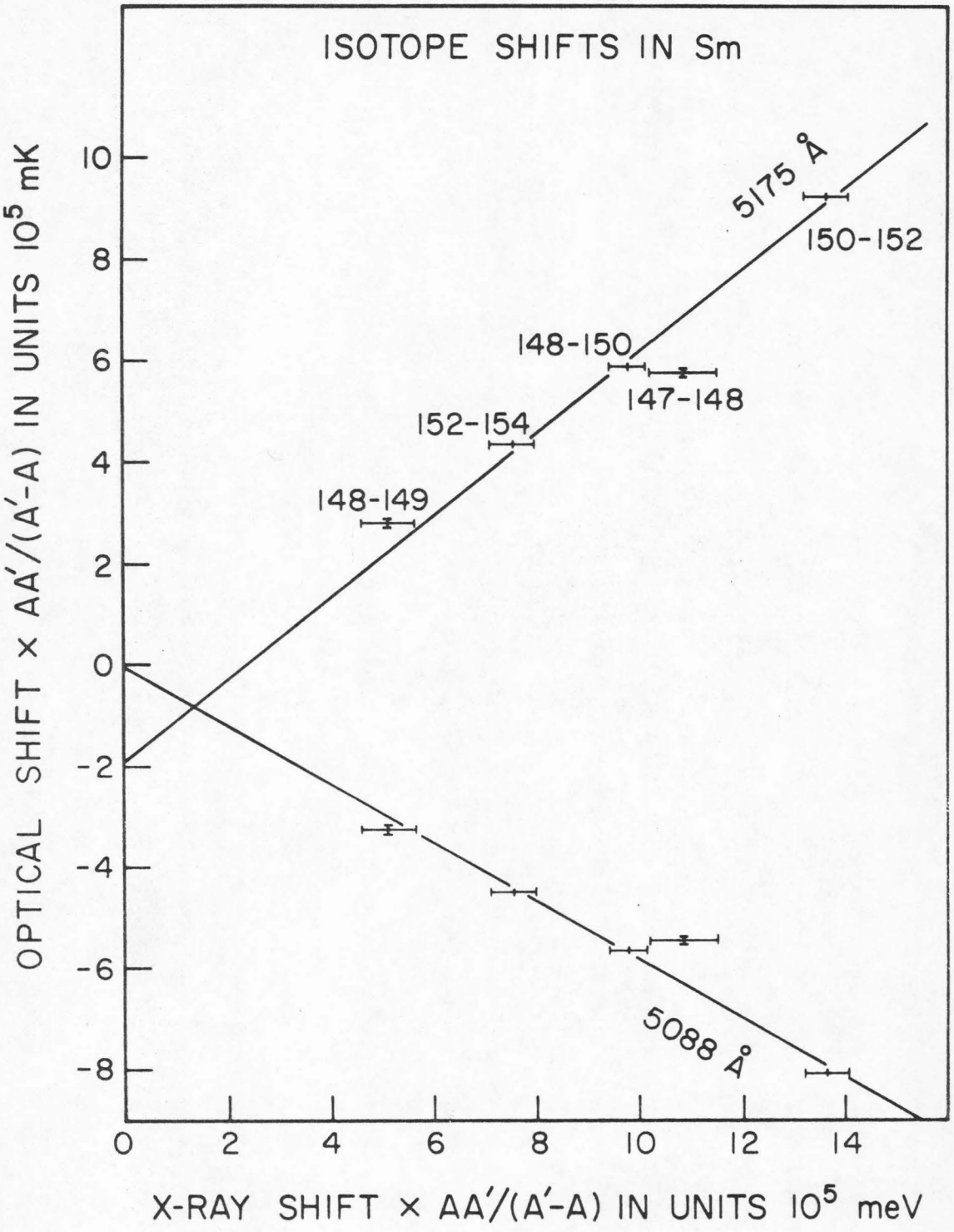
ISOTOPE SHIFTS IN Sm
OPTICAL SHIFT × AA′/(A′-A) IN UNITS 10⁵ mK
X-RAY SHIFT × AA′/(A′-A) IN UNITS 10⁵ meV
5175 Å
5088 Å
150-152
148-150
147-148
152-154
148-149
10
8
6
4
2
0
-2
-4
-6
-8
0
2
4
6
8
10
12
14

FIG. 7

Figure 8. Comparison of the x-ray volume shifts and the optical shifts in Pb.

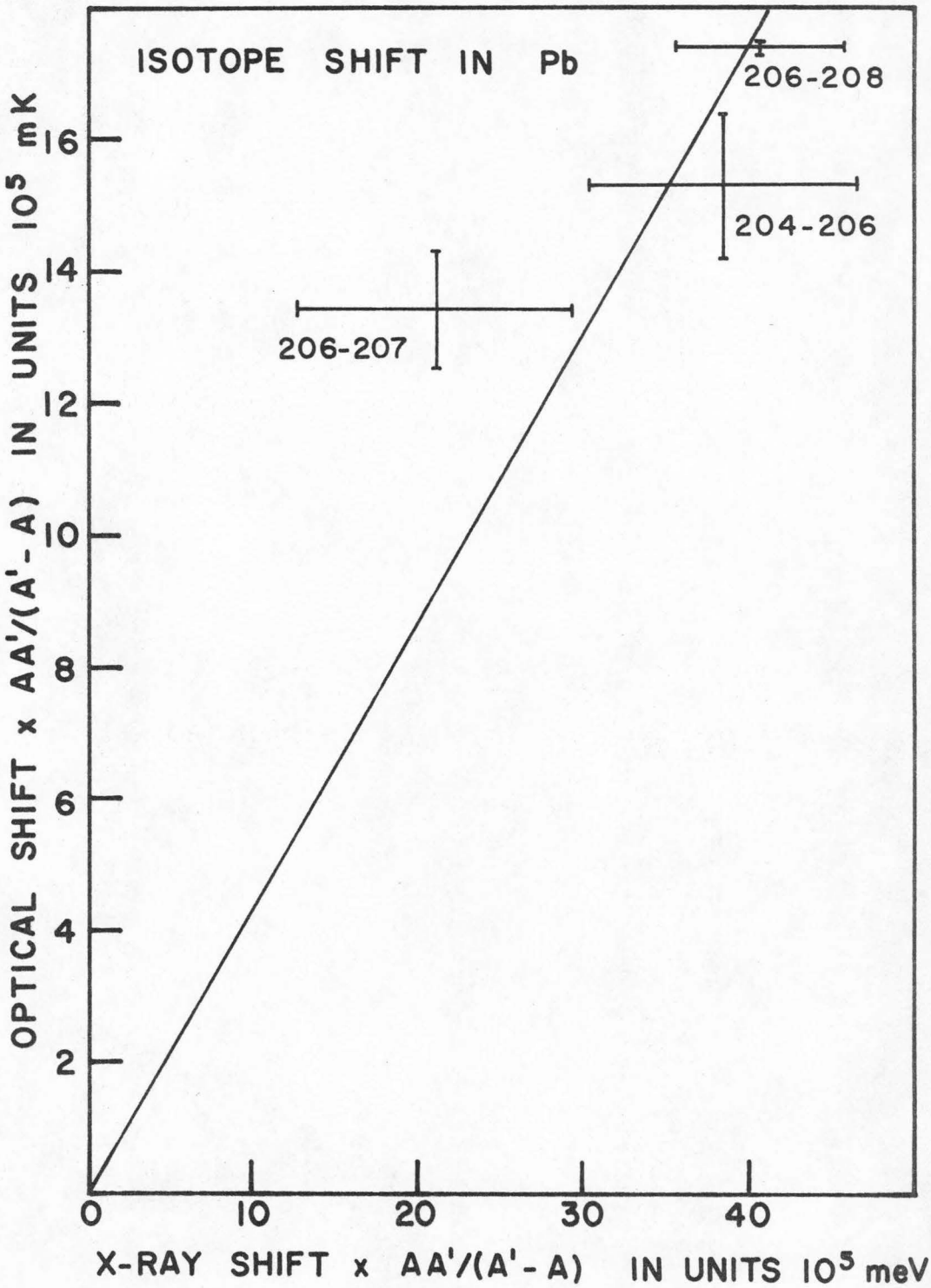
ISOTOPE SHIFT IN Pb
206-208
204-206
206-207
OPTICAL SHIFT x AA'/(A'-A) IN UNITS 10⁵ mK
2
4
6
8
10
12
14
16
0
10
20
30
40
X-RAY SHIFT x AA'/(A'-A) IN UNITS 10⁵ meV

FIG. 8

of Sm. The optical I.S. in Sm was also measured by Hansen et al[29]. The result of the least squares fitting is plotted for two optical lines in fig. 7. It is again evident that the odd nuclei do not fall on the straight line. The optical parameters C_1^i and M^i for five Sm lines are listed in Table 6.

For the case of Pb, Steudel[31] made the optical I.S. measurements using unenriched Pb. A plot of optical versus x-ray I.S. is shown in fig. 8. Because of the large uncertainties in the shifts, the optical parameters cannot be deduced. Assuming the mass shifts are small for Pb, we have drawn a line through the origin.

6.3 Comparison with Microscopic Models

The $\delta\langle r^2\rangle$ values from x-ray I.S. experiments provides a sensitive test for nuclear structure calculations. We compare our results with some of the microscopic nuclear model calculations.

Uher and Sorensen[32] have calculated $\delta\langle r^2\rangle$ values using the pairing plus quadrupole model. The nuclear system is divided into a core plus a few valence particles. Monopole polarization of the core by the particles is treated in a phenomenological manner by assuming that the particles interact independently with the core. Quadrupole polarization of the core by the

TABLE 7

The ratio of $\delta\langle r^2\rangle_{exp}$ to $\delta\langle r^2\rangle_{A^{1/3}}$ is compared to two theoretical predictions.

Isotope Pair	$\frac{\delta\langle r^2\rangle_{exp}}{\delta\langle r^2\rangle_{A^{1/3}}}$ This work	$\frac{\delta\langle r^2\rangle_{theo}}{\delta\langle r^2\rangle_{A^{1/3}}}$ Uher et al	$\frac{\delta\langle r^2\rangle_{theo}}{\delta\langle r^2\rangle_{A^{1/3}}}$ Krainov et al
$Nd^{142\ 144}$	1.38 ± 0.07	1.48	1.20
$Nd^{144\ 146}$	1.09 ± 0.15		1.20
$Nd^{146\ 148}$	1.21 ± 0.09	1.62	1.20
$Nd^{148\ 150}$	1.97 ± 0.07	2.31	1.20
$Sm^{148\ 150}$	1.44 ± 0.05	1.53	1.34
$Sm^{150\ 152}$	1.92 ± 0.06	2.26	1.34
$Pb^{204\ 206}$	0.54 ± 0.11	0.56	0.51
$Pb^{207\ 208}$	0.29 ± 0.12		1.35
$Pb^{206\ 208}$	0.55 ± 0.07		0.82

particles is estimated by using the B(E2) transition rates of even mass nuclei. The independent particle configuration of the valence nucleons is admixed by the pairing plus quadrupole interaction and the resulting wavefunctions are used to calculate isotope shifts of the charge radius. One of their findings is that the quadrupole effects contribute most to variations observed in isotope shifts throughout the periodic table. Table 7 lists the $\delta\langle r^2\rangle/\delta\langle r^2\rangle_{sph}$ values of our experiments and the calculation for Nd, Sm, and Pb.

In fig. 9 we have plotted $\delta E/\delta E$ of the even-even Nd I.S.'s and the values predicted by Uher and Sorensen. The trend of the variations is reproduced but the detailed agreement is still not good.

Also included in Table 7 and fig. 9 are the predictions by Krainov and Mikulinskii[33]. They have calculated the isotope shifts and quadrupole moments of nuclei neighboring to spherical ones on the basis of the nuclear theory developed by Migdal and Larkin[34] for finite Fermi Systems. Two parameters, one for the interaction between nucleons inside the nucleus and the other for nucleons on the surface, are introduced. There is only partial agreement in the case of Sm and Pb. As can be seen from fig. 9, our result in Nd contradicts their prediction.

Figure 9. X-ray I.S. versus model predictions for Nd.

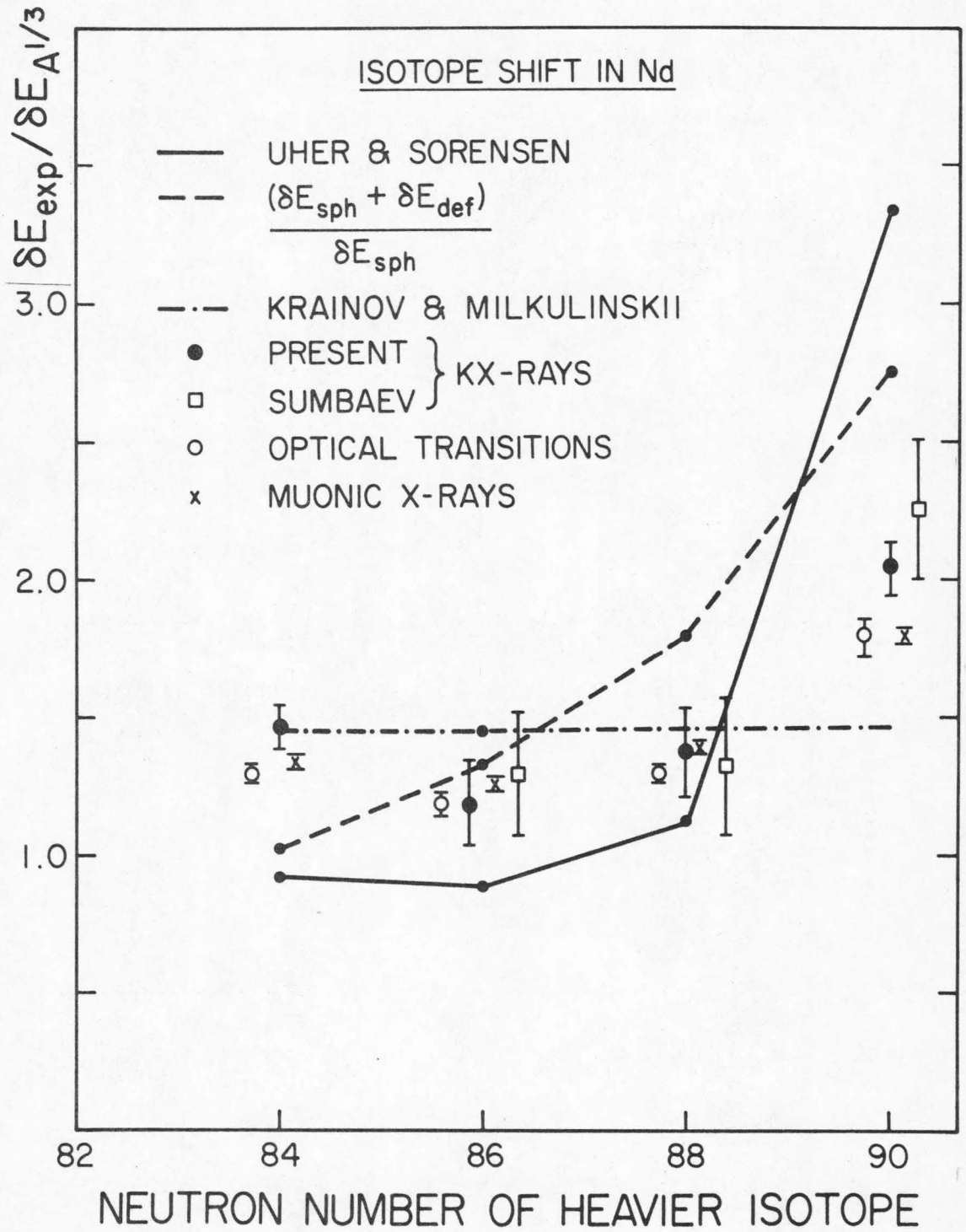
ISOTOPE SHIFT IN Nd
UHER & SORENSEN
$\frac{(\delta E_{sph} + \delta E_{def})}{\delta E_{sph}}$
KRAINOV & MILKULINSKII
PRESENT
SUMBAEV
KX-RAYS
OPTICAL TRANSITIONS
MUONIC X-RAYS
$\delta E_{exp} / \delta E_{A^{1/3}}$
3.0
2.0
1.0
82
84
86
88
90
NEUTRON NUMBER OF HEAVIER ISOTOPE

FIG. 9

Fig. 9 also has the values calculated for $(\delta E_{sph} + \delta E_{def})/\delta E_{sph}$ (eqn. 2.6 and 2.7). This simple minded static deformation model gives a much bigger value for Nd than our result.

6.4 Conclusion

The $\delta\langle r^2\rangle$ values for even-even Nd isotopes have been applied to the high energy electron scattering experiment on the even Nd isotopes by Heisenberg et al[35]. This has allowed a more precise determination of the mean charge radius values, $\langle r^2\rangle$, of the Nd isotopes. Greenlees et al[36] have shown that the mean square radius $\langle r^2\rangle$ of nuclei can be determined from elastic proton scattering using a reformulated optical model. Combining these results would yield the mean square radius of the neutrons.

One puzzling aspect of the isotope shift is the odd-even staggering effect. All I.S. experiments have shown that the change in the mean square charge radius when one neutron is added to a nucleus with even neutron numbers is always less than half of the $\delta\langle r^2\rangle$ when two neutrons are added, i.e.

$$\frac{\langle r^2\rangle_{N+1} - \langle r^2\rangle_N}{\frac{1}{2}\left\{\langle r^2\rangle_{N+2} - \langle r^2\rangle_N\right\}} < 1$$

There is no nuclear theory at present to explain this effect.

Bulk compressibility has not been able to explain the I.S. anomaly in the region of deformed nuclei. Fradkin[37] has introduced a deformation compressibility. Using two impirical parameters of regular compressibility $\eta = 0.7$ and deformation compressibility $\xi = 0.2$, the anomaly in the region of deformed nuclei is fairly well accounted for. So far, there is no microscopic nuclear theory for this effect.

The $\delta\langle r^2\rangle$ values from I.S. give a very valuable parameter for the nuclear structure. The phenomenological models which have been used so far can provide a guide. A more fundamental approach, perhaps a realistic Hartree Fock calculation, would be the next step.

APPENDIX I

SPECTROMETER CONTROL SYSTEM

The spectrometer control system (fig. 10) has the flexibility to scan repetitively an x-ray region of adjustable width for one to four isotope samples. The output from the NaI detector goes through a pre-amp., an amplifier and a single-channel analyser into a scaler. The scaler, scanner and master timer are connected in a daisy chain. The master timer is set to time 20 seconds in the master mode. To begin an experiment, the master timer is started by a push button. This allows the scaler to start accepting counts. At the end of 20 seconds, the master timer stops and the scanner transmits the counts on the scaler onto the magnetic tape unit. The scanner then resets the scaler and the master timer. The scanner is used in the external recycle mode and will recycle after the dead time timer has counted for 6 seconds. The scanner starts the master timer again and the whole sequence is repeated.

The gate from the master timer is connected to preset counter 1 and the isotope changing unit. After each 20 seconds counting interval, the master timer stops and the pulse from the gate activates the isotope changing unit. In arrangement I, the axis for the sample

Figure 10. Spectrometer control and data acquisition system.

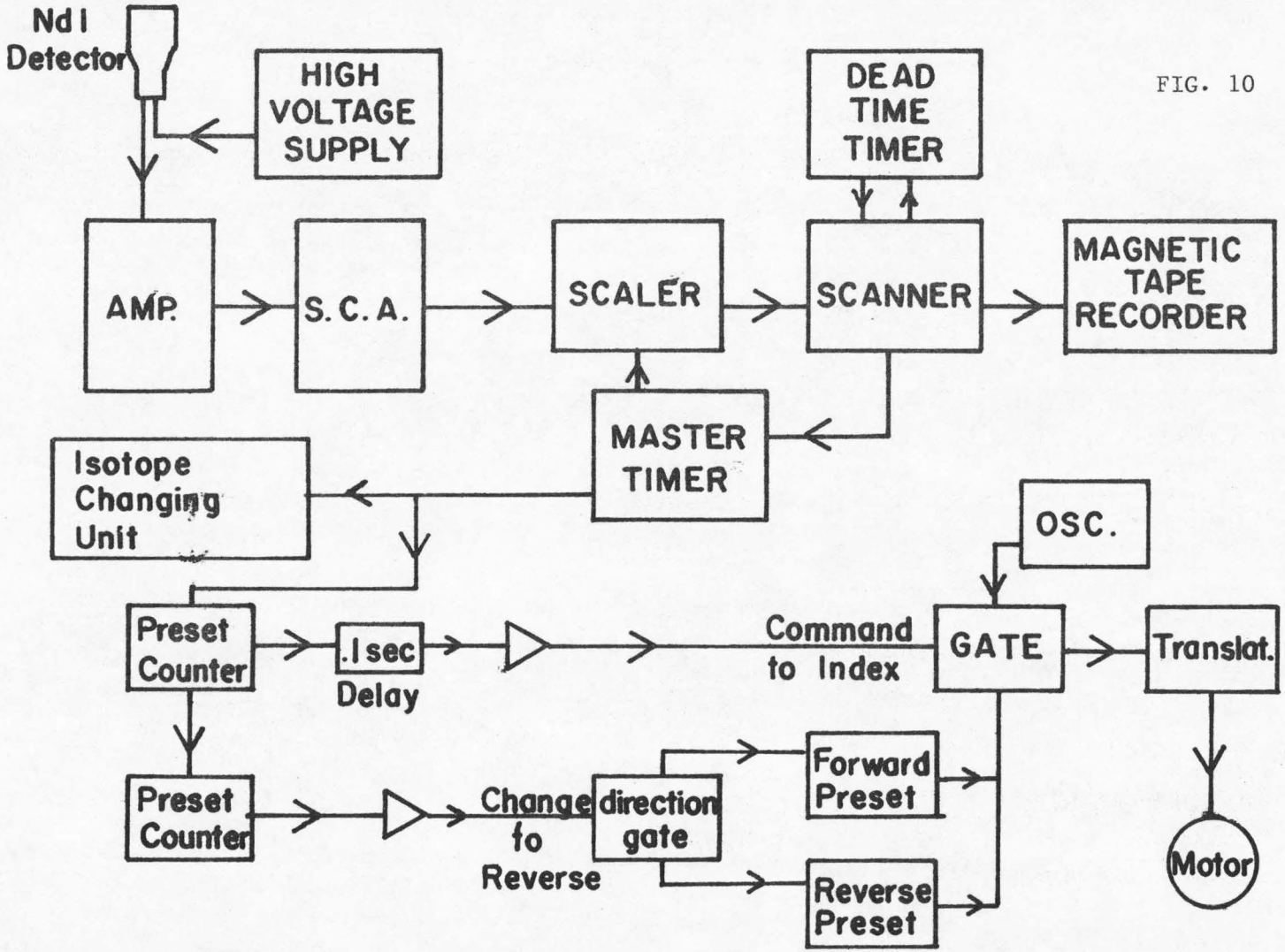

FIG. 10

SPECTROMETER CONTROL and DATA ACQUISITION SYSTEM

wheel has microswitch stops. The pulse from the gate will move the sample wheel from one isotope position to another. In arrangement II, the axis of the sample wheel is connected to a Slo-syn stepping motor. The pulse from the gate will index a Slo-syn Indexer. In either case, the net effect is that the sequence of gate pulses changes the isotopes in a sequential manner. For example, if we have three isotopes A, B, C, the isotopes will appear before the excitation source in the sequence A, B, C, A, B, C, A, B, ...

The gate pulse also goes to preset counter 1. This counter is preset to (n+1) if we are measuring n isotopes. After (n+1) gate pulses, the output of preset counter 1 gives a pulse to preset counter 2. The output is also used, after a 0.1 second delay (explained below), to give a command to index. This moves the stepping motor the number of steps specified in the forward preset. Thus, if we are measuring three isotopes A, B, C, the spectrometer remains in position 1 while we are taking the counts from isotope A, B, C and then A again. Then the spectrometer is moved to position 2 and we measure isotopes B, C, A and then B. This is the counting pattern given in Table 3.

Preset counter 2 controls the rewind of the spectrometer. It is set to the number of spectrometer

positions where we make measurements for the x-ray profile. The preset counter 2 gets a count every time preset counter 1 gives a pulse. After we have made all measurements in the last spectrometer position, preset counter 1 gives a pulse for command to index. It also makes preset counter 2 reach its preset. The output holds the direction gate to reverse. Since the command to index pulse is delayed for 0.1 seconds, the motor will be stepped in the reverse direction. To take care of backlash, the motor is made to overshoot and then approach the starting position in the forward direction.

All the motor movement and isotope change are done in the dead time interval.

APPENDIX II

PREPARATION OF ISOTOPE SAMPLES

After we have ascertained that the isotope sample has the correct crystal structure, we grind the sample to a fine powder form. We weigh out the appropriate amount of the isotope and mix it thoroughly with an organic substance.

The first organic substance we have used is teflon. An amount equal to half the mass of the isotope is used. The mixture is sandwiched between two hardened steel cylinders and the assembly is placed snugly inside a hollow cistern. This is pressed under 2×10^6 gm/cm^2 pressure (about 2000 atmospheres). The resulting pill is very strong.

However, it is quite difficult to recover the isotope after the experiment after it has been mixed with teflon. We have to burn the teflon away at high temperature. There is considerable loss of the isotopes.

We have used lucite powder as a substitute for teflon. To make a strong pill, we have to put the isotope-lucite mixture to about 200°C. This introduces uncertainties about the chemical purity of the isotope samples.

The best substance we have found for our purpose is Formvac. We form the pill in the same manner with

about half the amount by weight of Formvac. After the experiments, the Formvac is dissolved in Dichloro-ethane. The isotope settles to the bottom and is separated in a centrifuge.

APPENDIX III

ISOTOPIC COMPOSITION OF ISOTOPE SAMPLES

The isotope samples used are highly enriched samples. Table 8 gives the percentage composition of the samples used in the experiments. Since the enrichment is not 100%, the wavelengths measured correspond to a weighted average of the different isotopes present in the sample. The experimental shifts, therefore, have to be corrected. In cases where all the stable isotopes are measured, we can account for the isotopic composition in an exact way. If only some of the isotopes are measured, we have to make use of the relative optical shifts. But since the isotopic corrections are usually of the order of a few percent, this approximate treatment does not introduce appreciable error. We will outline the two procedures below.

Definition:

n = number of stable isotopes for the element

m = number of isotope samples used in the experiment

$\overline{\overline{C}}$ is a matrix where C_{ij} denotes the percentage of the j-th isotope present in the i-th isotope sample

$\bar{\lambda}$ is a N dimensional vector where λ_j denotes the true absolute wavelength of the j-th isotope. It is an unknown.

TABLE 8

Isotopic Composition of All Isotopes Used

Nd	142	143	144	145	146	148	150
142	96.24	2.06	0.99	0.24	0.33	0.08	0.06
143	2.41	91.06	4.43	0.39	1.50	0.14	0.09
144	1.65	2.00	90.10	3.47	2.39	0.25	0.15
145	0.93	0.59	2.53	91.82	3.66	0.29	0.15
146	0.43	0.20	0.70	0.69	97.46	0.32	0.13
148	1.32	0.63	1.32	0.63	1.97	93.31	0.84

Sm	144	147	148	149	150	152	154
147	<0.10	97.93	0.84	0.50	0.17	0.35	0.21
148	-	0.026	99.941	0.032	-	-	-
149	<0.08	0.33	0.55	97.46	0.65	0.70	0.30
150	<0.01	<0.01	<0.01	0.017	99.973	0.01	<0.01
152	<0.01	0.08	0.07	0.12	0.1	99.18	0.45
154	-	0.04	0.04	0.19	0.04	0.39	99.30

Gd	152	154	155	156	157	158	160
154	<0.10	66.95	17.42	7.16	3.13	3.47	1.88
155	<0.05	0.24	94.4	2.84	0.98	1.03	0.51
156	<0.01	<0.01	0.05	99.82	0.12	0.02	0.01
157	<0.02	0.07	0.64	1.66	93.7	3.11	0.83
158	<0.05	<0.05	0.25	0.56	0.81	97.58	0.81
160	<0.05	0.1	0.3	0.6	0.7	3.1	95.2

Dy	156	158	160	161	162	163	164
162	<0.01	<0.01	0.15	5.13	91.04	2.82	0.86
164	<0.02	<0.02	<0.02	0.40	1.34	5.55	92.71

Er	162	164	166	167	168	170
166	<0.005	<0.005	99.97	0.03	<0.01	<0.005
168	0.03	0.03	1.33	2.7	95.2	0.77
170	<0.1	<0.1	1.04	0.97	1.93	96.06

Hf	174	176	177	178	179	180
178	<0.05	0.22	1.54	94.72	1.84	1.69
180	<0.03	0.07	0.27	0.65	0.80	98.21

Pb	204	206	207	208
204	73.80	11.97	5.96	8.29
206	<0.01	99.77	0.21	<0.03
207	<0.02	2.16	92.4	5.48
208	0.07	1.15	0.82	97.98

$\bar{S}$ is a N dimensional vector where S_j denotes the relative optical I.S. for the j-th isotope.

$\bar{D}$ is a M dimensional vector where D_j denotes the measured x-ray I.S. between the i-th isotope sample and the first isotope sample. $D_1 = 0$.

α is the true absolute wavelength of the first isotope sample. $\alpha = \lambda_k$, where k is the enriched isotope in the first isotope sample.

Case 1.

In the case where all the stable isotopes are measured, we have n = m. The absolute wavelength of our i-th isotope sample is $(\alpha + D_i)$. This is equal to the weighted average of the wavelengths of the isotopes that the i-th sample is composed of.

$$\therefore \quad (\alpha + D_i) = \sum_j C_{ij} \lambda_j \qquad \text{(III.1)}$$

$$\therefore \quad \lambda_j = \sum_I (C^{-1}_{ji})(\alpha + D_i) - \alpha + \sum_i (C^{-1}_{ji}) D_i \qquad \text{(III.2)}$$

Therefore, the true I.S. between isotope j and k is

$$\lambda_j - \lambda_k = \sum_i (C^{-1}_{ji} - C^{-1}_{ki}) D_i \qquad \text{(III.3)}$$

Case 2

For $m < n$, we need the relative optical I.S. $\bar{S}$ which is related to $\bar{\lambda}$ by

$$\bar{\lambda} = a\bar{S} + b \qquad \text{(III.4)}$$

where a, b are unknown constants.

Suppose our i-th and j-th isotope samples are enriched with the p-th and q-th isotope, our measured shift is $D_i - D_j$ and the true shift between the p-th and q-th isotope is $\lambda_p - \lambda_q$. So we should correct our measured shift by the factor

$$\frac{\lambda_p - \lambda_q}{D_i - D_j}$$

To get this factor we write

$$(D_i - D_j) = \sum_r (C_{ir} - C_{jr})\, \lambda_r \qquad \text{(III.5)}$$

Putting eqn. (III.4) into (III.5) gives

$$(D_i - D_j) = \sum_r (C_{ir} - C_{jr})(aS_r + b)$$

$$= a\sum_r (C_{ir} - C_{jr})S_r + b\sum_r (C_{ir} - C_{jr})$$

The last term is zero by definition of $\bar{\bar{C}}$

$$\therefore \quad a = \frac{D_i - D_j}{\sum_r (C_{ir} - C_{jr}) S_r}$$

Putting this value of a into eqn. (III.4), we get

$$(\lambda_p - \lambda_q) = \frac{D_i - D_j}{\sum_r (C_{ir} - C_{jr}) S_r} (S_p - S_q)$$

Therefore the required correction coefficient is

$$\frac{\lambda_p - \lambda_q}{D_i - D_j} = \frac{S_p - S_q}{\sum_r (C_{ir} - C_{jr}) S_r}$$

APPENDIX IV

DETAILED RESULTS OF ALL MEASUREMENTS

Table 9 gives the result of measurements. Only the final results for 23 isotope pairs are presented in Chapter 5.

Since the final results have been obtained by a linear least squares fit of all measurements, the errors for the unlisted pairs are given by an error matrix. We present in Table 10 the complete result for Sm. The shift and error for any isotope pair of Sm can be read off from Table 10.

TABLE 9

Results of all measurements.

Isotope Pair	Mass Shift (meV)	Coulomb Shift δE (meV)
Nd_2O_3		
Nd 142-143	-0.7	21.0 ± 2.3
Nd 142-144	-1.3	68.9 ± 14.6
Nd 143-144	-0.6	48.0 ± 3.4
Nd 145-146	-0.6	44.6 ± 3.4
Nd 148-150	-1.2	93.0 ± 5.6
Nd 142-145	-2.0	74.1 ± 3.4
Nd 142-146	-2.6	125.4 ± 6.8
Nd 142-148	-3.9	189.8 ± 3.4
Nd 144-148	-2.5	120.8 ± 3.4
Nd 142-150	-3.8	298.9 ± 10.1
Nd 144-150	-3.7	215.6 ± 4.5
NdF		
Nd 142-146	-2.6	126.7 ± 4.8
Nd 146-148	-1.2	59.7 ± 5.4
Nd 148-150	-1.2	106.3 ± 5.3
Sm 147-148-149-150:		
Sm 147-148	-0.7	52.5 ± 4.4
Sm 148-149	-0.7	21.1 ± 3.6
Sm 149-150	-0.7	67.0 ± 4.6
Sm 147-152	-3.3	257.7 ± 5.8
Sm 149-150-152-154:		
Sm 149-150	-0.7	63.5 ± 3.9
Sm 150-152	-1.3	119.9 ± 3.7
Sm 152-154	-1.2	63.7 ± 4.3
Sm 148-154	-3.8	275.5 ± 3.5
Sm 147-148-149:		
Sm 147-148	-0.7	48.5 ± 3.9
Sm 148-149	-0.7	24.1 ± 2.9

TABLE 9 (Cont'd)

Results of all measurements.

Isotope Pair	Mass Shift (meV)	Coulomb Shift δE (meV)
Gd 154-157	-2.0	111.5 ± 14.3
Gd 154-158	-2.6	111.1 ± 8.6
Gd 155-156	-0.7	34.3 ± 5.4
Gd 155-157	-1.3	40.9 ± 4.0
Gd 155-160	-3.1	136.8 ± 4.2
Gd 156-158	-1.2	53.5 ± 5.1
Gd 156-160	-2.5	103.7 ± 4.6
Gd 157-158	-0.6	38.0 ± 5.1
Gd 157-160	-1.8	113.3 ± 10.5
Gd 158-160	-1.2	51.0 ± 4.7
Dy 162-164	-1.2	55.7 ± 4.3
Er 166-168	-1.3	69.5 ± 4.5
Er 168-170	-1.3	80.0 ± 6.1
Hf 178-180	-1.3	77.4 ± 5.3
$Pb(NO_3)_2$		
Pb 204-206	-1.3	269.4 ± 33.9
Pb 206-207	-0.6	34.8 ± 18.6
Pb 206-208	-1.3	174.6 ± 24.4
PbS		
Pb 204-206	-1.3	183.3 ± 38.7
Pb 206-207	-0.6	49.2 ± 19.8
Pb 206-208	-1.3	189.4 ± 23.7

TABLE 10

Result of Sm for all isotope pairs.

A \ A'	148	149	150	152	154
147	49.8 ±2.9	73.2 ±2.5	138.2 ±3.2	257.7 ±3.6	321.9 ±3.6
148		23.3 ±2.3	88.3 ±3.0	207.8 ±3.7	272.1 ±2.8
149			65.0 ±3.0	184.4 ±3.6	248.7 ±3.1
150				119.5 ±3.5	183.8 ±3.2
152					64.3 ±3.8

REFERENCES

1) P. Brix and H. Kopfermann, Rev. Mod. Phys. 30, 517 (1958).

2) D. N. Stacey, Rep. Progr. Phys. XXIX, 171 (1966).

3) C. S. Wu and L. Wilets, Ann. Rev. Nucl. Sci. 19, 527 (1969).

4) S. Devons and I. Duerdoth, Advances in Nuclear Physics 2, 295 (1969).

5) K. W. Ford and J. G. Wills, LASL Preprint LA-DC-11393 (1968).

6) R. T. Brockmeier, F. Boehm and E. N. Hatch, Phys. Rev. Letters 15, 132 (1965).

7) O. I. Sumbaev, E. V. Petrovich, V. S. Sykov, A. S. Rylnikov and A. I. Grushko, Yadern Fiz. 5, 544 (1967); [English transl.: Soviet J. Nucl. Phys. 5, 387 (1967)].

8) R. B. Chesler and F. Boehm, Phys. Rev. 166, 1206 (1968).

S. K. Bhattacherjee, F. Boehm and P. Lee, Phys. Rev. Letters 20, 1295 (1968).

S. K. Bhattacherjee, F. Boehm and P. L. Lee, Phys. Rev. 188, 1916 (1969).

P. L. Lee and F. Boehm, Phys. Letters 35B, 33 (1971).

9) E. J. Seppi, H. E. Henrikson, F. Boehm and J. W. M. DuMond, Nucl. Instr. Methods 16, 17 (1962).

10) P. L. Lee, F. Boehm and E. Seltzer (to be published).

11) G. Racah, Nature 129, 723 (1932).

12) J. Rosenthal and G. Breit, Phys. Rev. 41, 459 (1932).

13) M. S. Wertheim and G. Igo. Phys. Rev. 98, 1 (1955).

14) P. Brix and H. Kopfermann, Rev. Mod. Phys. 30, 517 (1958).

15) A. R. Bodmer, Proc. Phys. Soc. (London) A66, 1041 (1953).

16) E. E. Fradkin, Zh. Eksperim. i Teor. Fiz. 42, 787 (1962), Soviet Phys. - JETP 15, 550 (1962).

17) F. A. Babushkin, Opt. i Spectoskopia 15, 721, Opt. Spectry. (USSR) 15, 393 (1963).

18) E. C. Seltzer, Phys. Rev. 188 No. 4, 1916 (1969).

19) J. Bauche, Compt. Rend. 263, 685 (1966).

20) R. B. Chesler, F. Boehm and R. T. Brockmeier, Phys. Rev. Letters 18, 953 (1967).

21) F. Herman and S. Skillman, Atomic Structure Calculation (Prentice Hall, Inc., Englewood Cliffs, N. J. 1963).

22) J. P. Vinti, Phys. Rev. 56, 1120 (1939).

23) O. I. Sumbaev and A. F. Mezentsev, Soviet Phys. JETP 21, 295 (1965).

24) P. H. Stelson and L. Grodzins, Nuclear Data 1, No. 1, 27 (1965).

25) R. B. Chesler and F. Boehm, Phys. Rev. 166, 1206 (1968).

26) O. I. Sumbaev, Nuclear Structure, Dubna Symposium 1968, 527, IAEA, Vienna, 1968.

27) C. W. E. Van Eijk and M. J. C. Visscher, Phys. letters, 34B, 349 (1970).

28) C. W. E. Van Eijk and F. Schutte, Nucl. Phys. A151, 459 (1970).

29) J. E. Hansen, A Sterdel and H. Walther, Z. Physik, 203, 296 (1967)

30) A. Faessler and H. Walther in Premiere Reunion Annuelle de L'Association Europeene de Spectroscopie Atomique, Paris, 1969 (unpublished).

31) A. Steudel, Z. Physik 133, 438 (1952).

32) R. A. Uher and R. A. Sorensen, Nucl. Phys. 86 1, (1966).

33) V. P. Krainov and M. A. Mikulinskii, Yadern Fiz. 4, 928 (1966); [English Transl.: Sov. J. Nucl. Physics 4, 665 (1967)]

34) A. B. Midgal and A. I. Larkin, Soviet Phys. JETP 18 717 (1964).

35) J. H. Heisenberg, J. S. McCarthy, I. Sick and M. R. Yearian, Nucl. Phys. A164, 340 (1971).

36) G. W. Greenlees, G. T. Pyle and Y. C. Tang, Phys. Letters 26B, 11; Phys. Rev. 171, 1115 (1968).

37) E. E. Fradkin, Soviet Phys. JETP 15, 1550 (1962).